Int. J. Nav. Archit. Ocean Eng. (2013) 5:614~624
http://dx.doi.org/10.2478/IJNAOE-2013-0157
pISSN: 2092-6782, eISSN: 2092-6790

Heaving displacement amplification characteristics of a power buoy in shoaling water with insufficient draft

Hyuck-Min Kweon[1], Il-Hyoung Cho[2] and Hong-Yeon Cho[3]

[1]*Department of Railway Construction and Environmental Engineering, Gyeongju University, Gyeongbuk, Korea*
[2]*Department of Ocean System Engineering, Jeju National University, Jeju, Korea*
[3]*Principal Research Scientist, Marine Environments & Conservation Research Department, Korea Institute of Ocean Science & Technology, Gyeonggi, Korea*

ABSTRACT: *The resonance power buoy is a convincing tool that can increase the extraction efficiency of wave energy. The buoy needs a corresponding draft, to move in resonance with waves within the peak frequency band where wave energy is concentrated. However, it must still be clarified if the buoy acts as an effective displacement amplifier, when there is insufficient water depth. In this study, the vertical displacement of a circular cylinder-type buoy was calculated, with the spectrum data observed in a real shallow sea as the external wave force, and with the corresponding draft, according to the mode frequency of normal waves. Such numerical investigation result, without considering Power Take-Off (PTO) damping, confirmed that the area of the heave responses spectrum can be amplified by up to about tenfold, compared with the wave energy spectrum, if the draft corresponds to the peak frequency, even with insufficient water depth. Moreover, the amplification factor of the buoy varied, according to the seasonal changes in the wave spectra.*

KEY WORDS: Resonance power buoy; Energy extraction efficiency; Draft depth; Mode frequency; PTO.

INTRODUCTION

Wave energy extraction makes up a renewable energy sector, and its commercialization and real sea verification are being actively performed worldwide. Its most studied area is the point-absorber-type hydrokinetic power system. The absorber-type hydrokinetic energy extraction equipment normally uses a buoy, which is called a *power buoy*. It is known that an economic volume of hydrokinetic power can be extracted, as the amplitude increases when the power buoy moves in resonance with the waves.

There have been many researches regarding the performance of a point absorber as wave energy converter since 1970s. Mostly, they take advantage of large resonant motions of a floating buoy and the electricity is generated by hydraulic PTO system or linear generator system. Budal and Falnes (1975), French (1979), and French and Bracewell (1995) studied a small heaving buoy in waves for extracting wave energy. They found that energy can be absorbed from a sizable width of wave crest much larger than the diameter of the buoy if using the resonant motion of a floating buoy. Falnes (1999) proposed a two-object hydrokinetic power generation system that consisted of inner and outer buoys, and was designed to easily acquire energy, by maximizing the relative vertical motions when resonance occurred, as the natural frequency of the inner buoy corresponded

Corresponding author: *Hyuck-Min Kweon*, e-mail: *choiziwon@hanmail.net*

with the mode frequency of the real sea area, where the system was installed. In addition, Grilli et al. (2011) verified, through tests and numerical calculations, that the energy extraction efficiency increased from the SPAR-type buoy and three satellite buoys with different heights that were moving around the resonance area, and suggested a measure for adjusting the natural frequency of the system for the safety and resonance of the hydrokinetic power generation system, through a combination of the main buoy and satellite buoys. Kweon et al. (2013a) have proven, through a systematic experiment, that the resonance buoy was amplified up to 5.66-fold in the amplitude ratio. As a linear generator is mounted on this resonance buoy, two movers operate according to the heaving displacement amplitude in this system.

Deep sea energy production increases the cost of transporting electricity to land, and an area with relatively smaller wave energy causes power generation economic feasibility problems. To overcome such problems, the increased displacement of the water level caused by the superposed waves that are reflected by the front surface of the breakwater installed in a small-sized fishing port can be used. However, low depth has insufficient water depth to produce resonance in the peaked frequency band, where the wave energy is concentrated. Therefore, the amplification of the heaving displacement of the power buoy must be verified. In this study, the waves that occurred during the entire period, regardless of whether or not big waves attack them, are called normal waves, and were used to investigate the resonance characteristics of the buoy.

This study investigates the amplitude effects of the heaving displacement of the power buoy, which needs to produce power constantly in low depth, where sufficient resonance depth cannot be secured, through a time-domain numerical simulation from the wave energy spectrum.

WAVE OBSERVATION AND CORRELATION ANALYSIS OF WAVE DATA BY MONTH

In this study, real sea data were analyzed, to simulate the motions of the power buoy. The analysis was performed on the heaving displacement of the superposed waves reflected by the front surface of the breakwater, as described in Section 1. As such data correspond to the normal waves, they are considered appropriate for investigating the amplitude characteristics of the power buoy, which was installed for continuous power generation.

Wave observation

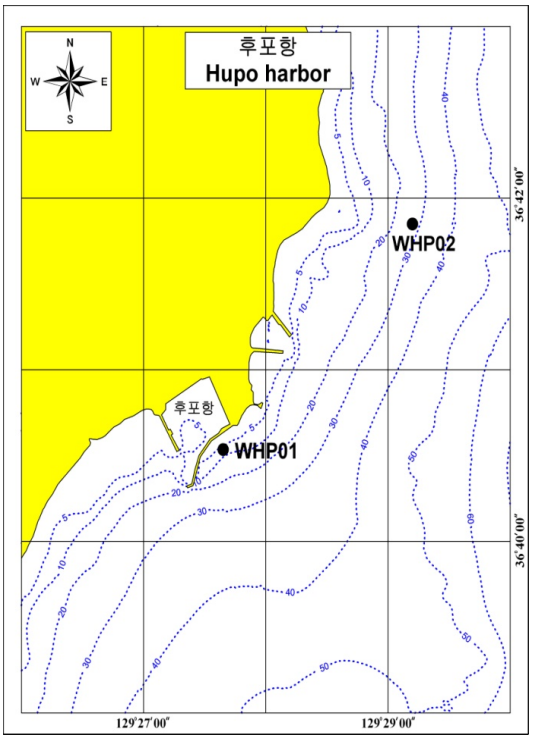

Fig. 1 Wave measurement stations around Hupo Port.

This study examines the wave data obtained around the eastern and northern coasts of Hupo Port in Uljin-gun, Gyeongsangbuk-do, South Korea (see Fig. 1), by using a wave and tide gauge (WTG). The wave observation started at the designated point, WHP01 (129°27'40"E, 36°40'35"N, with a water depth of about 10 *m*), on April 26, 2002, to investigate the wave conditions for the optimum design of the seawater exchange facility. The designated point was changed to WHP02 (with a water depth of about 18.5 *m*) in May 2005, and the observation has continued to this date. In this study, the data collected for three years from May 2002 to March 2005 were analyzed. The data at the WHP01 point are focused on.

For the data analysis, first, the pressure data that were measured continuously at 0.5 *sec* intervals were selected by 2,048 items every 30 *minutes*, and the pressure spectrum was calculated using the Fast Fourier Transform (FFT) technique. Then the pressure spectrum was converted to the wave energy spectrum, by applying the wave pressure - wave height spectrum transfer function that was obtained from the linear wave theory, and was used to calculate the waver property factors, including the significant wave height, peak period and mean period. The wave energy spectrum of the data that were measured at 0.5 *sec* intervals was presented with 60 components, at the 1/128 *Hz* interval between 5/128 *Hz* and 64/128 *Hz*.

Correlation analysis of the wave data by month

To design the resonance power buoy for electric power production, the wave period and wave height variations have to be predicted, to set the dimensions of the power buoy according to the target power production. However, multiple numbers of power buoys are needed for areas where the seasonal period and the wave height variations are distinct, and the power buoys must be installed based on such predictions. Meanwhile, separate examination of each monthly period would require 12 power buoys with different dimensions, which is economically unfeasible. In addition, the extraction efficiency of one buoy may differ depending on the seasonal period, and the difference in the wave height. That is, as the regional factors of the seasonal waves dominantly affect the extraction efficiency, rather than the performance of the power buoys, they create a problem with the design.

Considering the aforementioned problems, in this study, the buoy dimensions that caused the waves to be separated from the seasonal wave variations according to their similarity were determined, and the extraction rate of each corresponding wave was calculated separately. To achieve these, a relative correlation analysis was conducted in areas where the variations in the seasonal wave characteristics were comparatively distinctive. To investigate the correlation of waves all year around, the observation data that were obtained in the real sea located at 129°27'40"E, 36°40'35"N with a water depth of about 10 m for about three years from May 2002 to March 2005 were analyzed.

The wave characteristic data were divided into the monthly data (that comprised a total of 12 sets); the information on the wave height, peak period, average and estimated wave force of the divided data were normalized (mean = 0 and variance = 1), as shown in Table 1; a cluster analysis was conducted on the normalized data using the Euclidean distance (the mathematical distance of the normalized information), without assigning the weighted value number according to the correlation of the data; and the data were reconstructed into three sets of clustered data. The constructed data were regrouped into Group 1 (the data for November, December, January and February), Group 2 (for March, April, September and October) and Group 3 (for May, June, July and August).

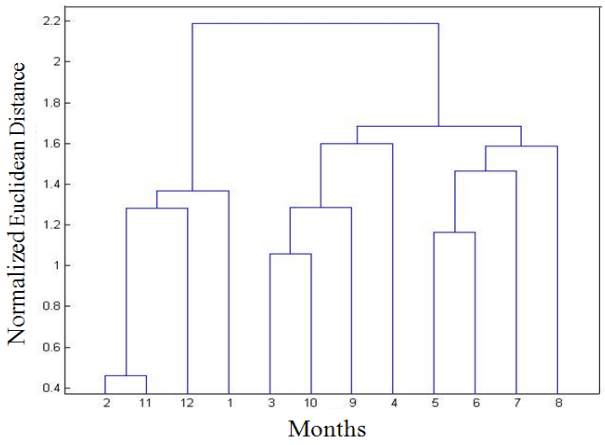

Fig. 2 Classification of the monthly wave data (dendrogram).

Table 1 Monthly variations in the wave characteristics and power (according to Kweon et al., 2013b).

	Significant wave height H_s (m)			Peak Wave Period T_p (s)			Mean Wave Period T_z (s)			Power (kW/m)
Month	Mean	R.M.S.	Mode	Mean	R.M.S.	Mode	Mean	R.M.S.	Mode	-
Jan	0.72	0.85	0.35	8.65	8.89	8.69	6.79	6.88	6.61	2.92
Feb	0.66	0.78	0.36	7.78	8.01	7.76	6.18	6.26	6.47	2.25
Mar	0.62	0.75	0.33	6.88	7.17	6.71	5.68	5.77	5.28	1.90
Apr	0.58	0.72	0.28	6.21	6.49	4.63	5.23	5.32	4.57	1.59
May	0.39	0.49	0.23	5.60	5.75	4.39	5.09	5.13	4.74	0.70
Jun	0.37	0.46	0.16	5.89	6.11	4.42	5.23	5.30	4.77	0.65
Jul	0.43	0.53	0.17	6.30	6.49	5.54	5.41	5.47	5.27	0.89
Aug	0.51	0.66	0.19	6.10	6.31	4.47	5.32	5.39	5.16	1.36
Sep	0.62	0.80	0.27	6.54	6.76	5.97	5.50	5.57	5.05	1.98
Oct	0.56	0.69	0.30	7.13	7.41	7.03	5.80	5.89	5.53	1.65
Nov	0.63	0.78	0.37	7.66	7.93	7.80	6.14	6.22	6.24	2.24
Dec	0.70	0.82	0.32	8.17	8.38	7.86	6.49	6.56	6.53	2.60
Mean	0.57	0.69	0.28	6.91	7.14	6.27	5.74	5.81	5.52	1.73

SPECTRUM ANALYSIS BASED ON CORRELATION ANALYSIS

The wave observation was discontinuously conducted at certain intervals in the real sea area. Therefore, the frequency spectrum can be analyzed using the time series data on the water level elevation for each data set, and this study intends to obtain the mean spectrum for all the data sets. The mean spectrum can be obtained using this method: the corresponding frequency energy according to each frequency for the entire set is aggregated, divided by the number of sets, and applied to the whole frequency-domain. The mean spectrum of the estimated spectrum $S_k(f_i)$ from the observation data was calculated as follows. The mean spectrum, $S_k(f_i)$, can be calculated from $S_k(f_i)$ as follows:

$$\overline{S(f_i)} = \frac{1}{N_T}\sum_{k=1}^{N_T} S_k(f_i) \tag{1}$$

where, $k = 1, 2, ..., N_T$ (N_T: total number of data sets) and $f_i = (i+4)/128\,Hz$, $i = 1, ..., 60$.

To express the normal wave spectrum, the Generalized Extreme Value (GEV) Cumulative Distribution Function (CDF) proposed by Kweon et al. (2013b) was converted to the probability density function (pdf), and the following equation that is marked with the conversion factor was used:

$$S_f(f;\mu,\sigma,\xi) = \frac{k}{\sigma}\left[1+\xi\left(\frac{f-\mu}{\sigma}\right)\right]^{(-1/\xi)-1} exd\left\{-\left[1+\xi\left(\frac{f-\mu}{\sigma}\right)\right]^{-1/\xi}\right\} \tag{2}$$
$$1+\xi(f-\mu)/\sigma > 0$$

where, μ refers to the location parameter; $\sigma > 0$, the scale parameter; and ξ, the shape parameter. The conversion coefficient k is the coefficient that converts the aggregate of the normal wave spectrum surfaces to the aggregate of the mean spectrum surfaces, as described in the following equation:

$$1/k = 1/\left(\sum_{i=1}^{n} \overline{S(f_i)}\right)_{obs} df \tag{3}$$

where, the subscript *obs* refers to the observation value, and n, to the number of the equal frequency divisions for the calculation of the spectrum surface, which was set at 60 for this calculation. df was set at 0.0078125 (= 1/128).

On the other hand, the Gamma PDF, which was selected as another spectrum function candidate, is described in the following equation, which is expressed with two parameters:

$$S_f(f;\kappa,\theta) = \frac{k}{\theta^{\kappa}} \frac{1}{\Gamma(\kappa)} f^{\kappa-1} e^{-\frac{f}{\theta}} \qquad for\ f \geq 0\ and\ \kappa,\ \theta > 0 \tag{4}$$

where, θ refers to the scale parameter, and κ, to the shape parameter. As Eq. (4) is also a PDF, the total surface area is one (1). Therefore, the conversion coefficient k (which is the same as the definition of Eq. (3)) is needed to express the observed spectrum.

The group-averaged spectrum was calculated using the clustered data described in Section 2, and the parameters of the GEV and Gamma functions were estimated for each mean spectrum. The estimation technique was used with the maximum likelihood method, and the estimated parameters are presented in Table 2. On the other hand, the wave information such as the significant wave height and the peak period was deduced from the mean spectrum of the classified data.

Table 2 Parameter estimates of the normal wave spectrum.

Classification	H_s	T_p	Conversion coefficient, k	GEV-1 (ξ)	GEV-2 (σ)	GEV-3 (μ)	Γ-1(κ)	Γ-2(θ)
Group 1	0.807	8.533	1/24.58	0.020	0.038	0.118	8.783	0.016
Group 2	0.740	8.533	1/29.20	-0.011	0.041	0.130	9.363	0.016
Group 3	0.646	7.111	1/38.34	0.109	0.072	0.167	4.931	0.044
Total	0.725	8.533	1/30.47	0.180	0.050	0.132	5.498	0.031

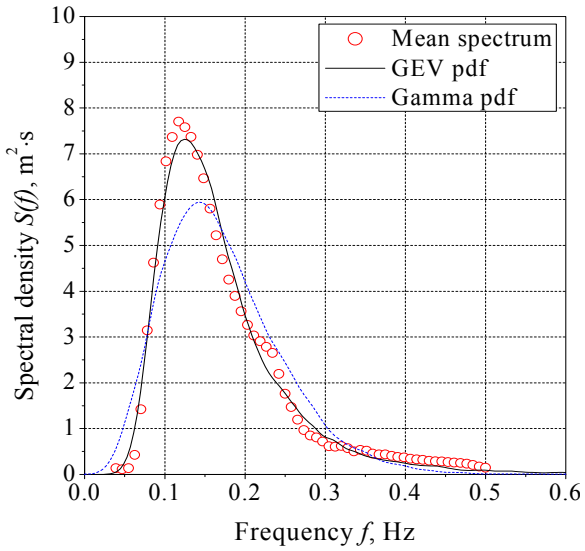

Fig. 3 Mean spectrum fitting for the annualtotal data.

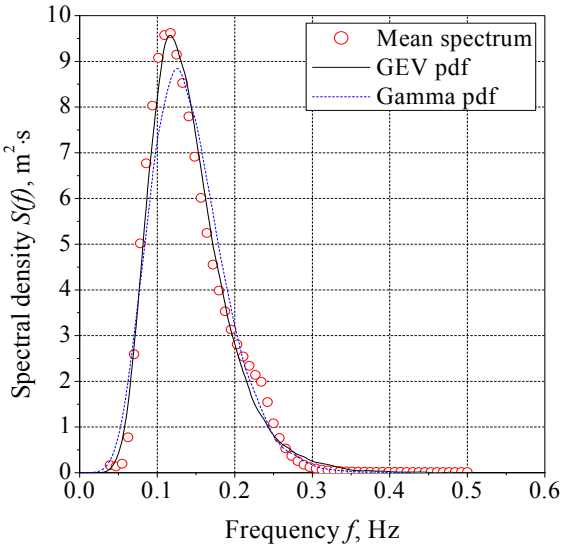

(a) Group 1.

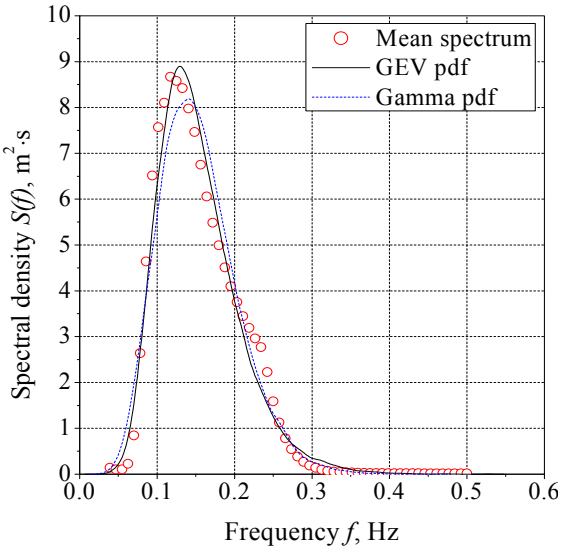

(b) Group 2.

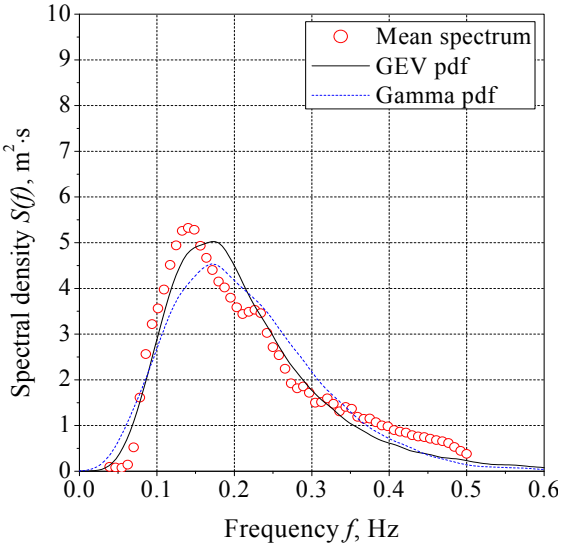

(c) Group 3.

Fig. 4 Mean wave spectrum fitting with the GEV and Gamma pdf.

COMPARISON AND ANALYSIS OF THE POWER BUOY MOTIONS

The dimensions of the resonance power buoys can be easily decided from the wave frequency spectrum for the design resonance frequency. However, the existing spectrum types have limits in expressing the normal waves, and in this study, the mode frequency spectrum of the waves that were observed year-round was analyzed. The resonance frequency of the power buoy was selected from the mode frequencies of the generated waves, and used to decide on the draft, from among the buoy dimensions. To compare and analyze the influence according to the spectrum type of the incident waves, the heaving motions of the numerical model buoy were calculated as examined by Kweon et al. (2013a). In this study, the reductions in the motions of the buoy due to actual PTO system by linear generator were not considered. The effect of actual PTO system on the motion of a floating buoy has been investigated by Cho et al. (2012).

Estimation of the mode frequency spectrum

For maximum power extraction, the corresponding resonance design according to the peak frequencies in Fig. 2 is required; but an examination would be needed to decide on the design resonance frequency, as the mode and peak frequencies of the

normal waves are different, as shown in the results of the study of Kweon et al. (2013b). The mode spectrum estimation differs from the arithmetic mean, because it is based on the occurrence frequency of the spectrum. To retain each observed spectrum, even from the aspect of the frequency of occurrence, the spectrum size was normalized as follows, by dividing it by the spectrum surface:

$$N_{S_K}(f_i) = S_k(f_i) / \sum_{i=1}^{n} S_k(f_i) df \tag{5}$$

where, n refers to the frequency for the calculation of the spectrum surface area, which is 60 in this calculation; $S_k(f_i)$, the spectrum size; df, the separated size of the spectrum (= 1.124 Hz); and $N_{S_K}(f_i)$, the normalized spectrum. The arithmetic mean value of the preceding normalized equation can be calculated as follows:

$$\overline{N_s(f_i)} = \frac{1}{N_T} \sum_{k=1}^{N_T} N_{S_K}(f_i) \tag{6}$$

where, N_T refers to the number of data for two years and 11 months, which in this case is 51,012. Fig. 3 shows the distribution of the arithmetic mean values of the spectrum that was normalized according to Eq. (5), the data for which were collected at the front surface of the northern breakwater of Hupo Port and analyzed every 30 *minutes*.

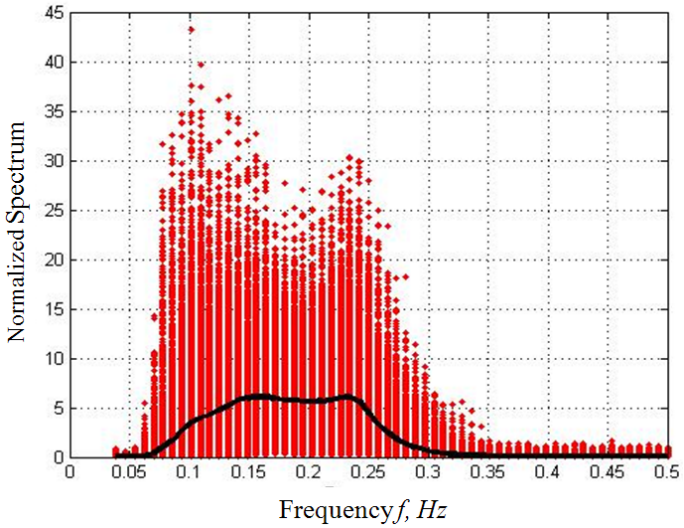

Fig. 5 Normalized spectrum of Hupo Port.

The normalized spectrum appears as two mountains, the representative values of which can be connected with the black line as shown in Fig. 5, while considering the spectrum as the density of the spectrum. The variations in the representative values show a flat shape between the frequencies of 0.15 *Hz* and 0.25 *Hz* (the 4.0-6.7 *sec* band). That is, the normalized spectrum distribution is characterized as not having exceptional peak values in the arbitrary frequency-domain.

Decision on the power buoy dimensions

The power buoy is an effective wave-power extraction device that uses the resonance phenomena with incident waves. Therefore, for effective extraction, the buoy must be designed so that the natural frequency may coincide with the peak frequency of the incident wave spectrum. The draft (*d*) in a cylinder-type buoy can be calculated as follows after ignoring the anticipated small heave added mass effect.

$$d = \frac{g}{\omega_h^2} \tag{7}$$

where, g (= 9.81 *m/sec*^{2}) refers to the gravity acceleration, and ω_h, to the buoy's heave natural frequency.

Had the natural frequency of the power buoy been designed to coincide with the peak frequencies of the normal wave spectrum in Groups 1, 2 and 3, the power buoy drafts would have appeared as 20.02, 15.32 and 10.64 m in each group, respectively. However, as the power buoy was installed at point WHP01 in low depth (less than 10 *m* deep), as shown in Fig. 1, such draft is considered inappropriate. Therefore, the buoy dimensions were set after considering the limit of the water depth and the frequency mode band of 0.15 *Hz* and 0.25 *Hz* in Fig. 5, in this study. Fig. 6 shows a conceptual drawing of the power buoy, and Table 3, its dimensions.

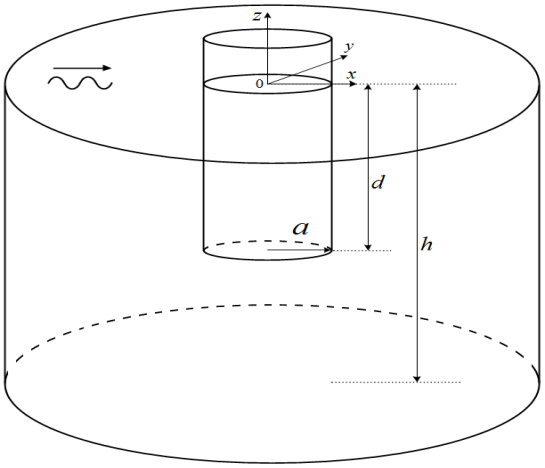

Fig. 6 A conceptual diagram of the power buoy.

Table 3 Specifications of the power buoy.

Properties	Depth (*m*)	Radius (*m*)	Draft (*m*)	Buoy mass (*kg*)	Heave natural frequency (*rad/sec*)
Values	10.0	1.5	6.0	43,472	1.17

Motion response of the power buoy

To investigate the amplification effects of the heaving motions when the power buoy was tuned to resonance with the incident waves, a time-domain motion analysis was conducted on the normal-wave-spectrum Groups 1, 2 and 3 proposed in the previous section. The hydrodynamic force (added mass, radiation damping coefficients) and wave exciting force of the power buoy that were needed to conduct the time-domain analysis were calculated in the frequency-domain, and the commercial AQWA code based on the boundary element method was used in this study. As the viscous effects were not considered in the commercial code, the viscous damping coefficient (b) had to be considered, and applied as follows, after estimating the non-dimensional viscous damping coefficient (κ) through the free-decay test after separating radiation damping effect. The non-dimensional viscous damping coefficient ($\kappa = 0.0233$) was used at the present calculation, as proposed by Kweon et al. (2013a), which was calculated as follows:

$$b = \frac{2\kappa\rho g A_w}{\omega_h} \tag{8}$$

where, A_w is the area of the water plane.

Fig. 7 shows the results of frequency-domain analysis for the models presented in Table 3. Each graph represents the Response Amplitude Operator (RAO), wave exciting force, added mass and radiation damping coefficient of the heave motion. As

shown in Fig. 7(a), the buoy tends to follow the waves as the frequency decreases; the RAO ($=|z/A|$) value becomes 1.0. The RAO increases while moving toward the resonant frequency band. The power buoy shows the maximum amplification factor at the resonance frequency, the value of which appears as about sevenfold. The heave RAO decreases suddenly in the high frequency region, after passing the resonance frequency band.

The time-domain equation for the heaving motion of the power buoy was derived from Newton's second law, and can be described as follows. $K(\tau)$ in the Eq. (9) is calculated from the radiation damping coefficients obtained from the frequency-domain analysis, and is called the *memory function* or the *retardation function,* because it considers the influence of the past motions of the buoy on the present. M_b refers to the mass of the power buoy; a_∞, the added mass at infinite frequency; and F_{ex}, the wave exciting force. Moreover, z represents the vertical displacement of the buoy. The equation of motion in the time-domain can be integrated numerically, using the 4-th order Runge-Kutta method.

$$\left(M_b + a_\infty\right)\ddot{z}(t) + b\dot{z}(t) + \int_0^t K(\tau)\dot{z}(t-\tau)d\tau + \rho g A_w z(t) = F_{ex}(t) \tag{9}$$

where, $K(\tau) = \frac{2}{\pi}\int_0^\infty b(\omega)\cos(\omega\tau)d\omega$.

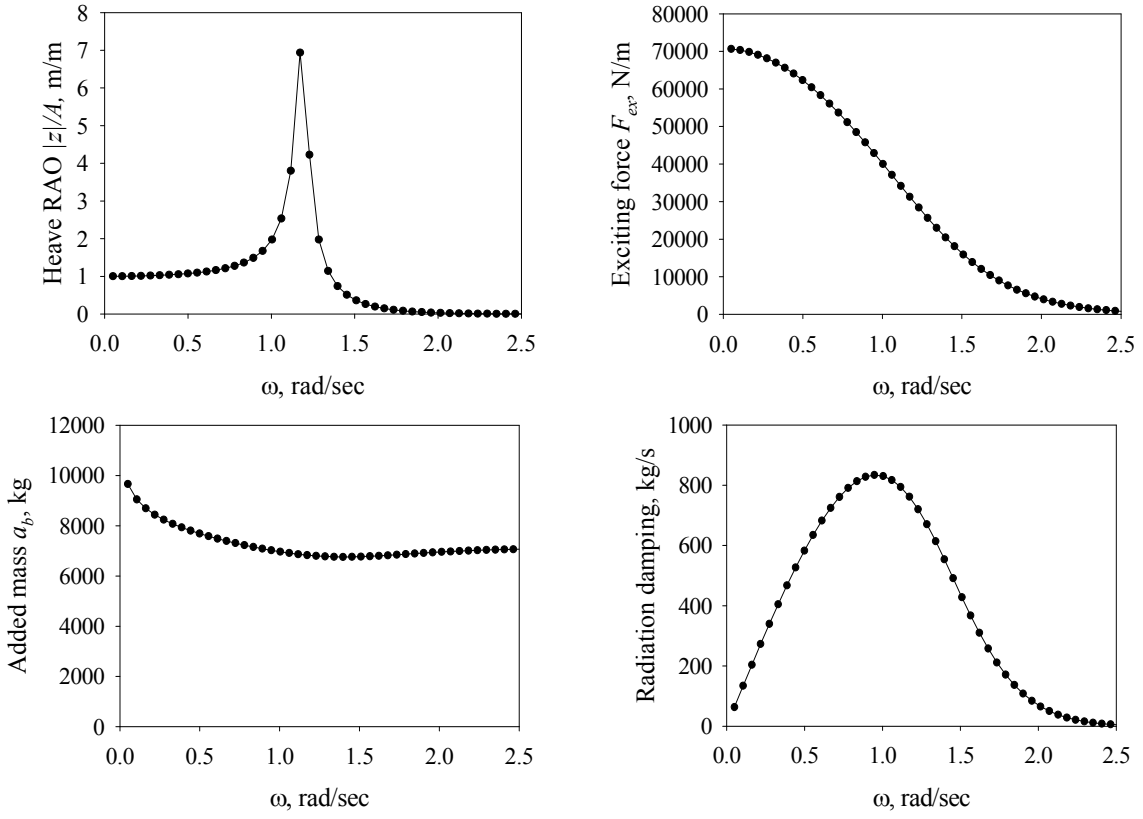

Fig. 7 Hydrodynamic results of the power buoy using AQWA in the frequency-domain.

Comparison of the heave RAO of the power buoy

The results of the time-domain analysis for the normal-wave Groups 1, 2 and 3 spectra described in Chapter 3 are presented in Figs. 8-10, respectively. Figs. 8-10(a) show the time series data on the wave elevation and heave motion of the buoy for the normal-wave Groups 1-3 and Figs. 8-10(b), the spectra obtained from applying the Fast Fourier Transform (FFT) technique on the time series data. Groups 1-3 showed that the heave motion of the power buoy tuned to resonance with the incident waves were largely amplified. To calculate the representative values (SWH: significant wave height and SBH: significant buoy height) in irregular waves, the SWH and the SBH of the power buoy were calculated by applying the zero-crossing method to the time series data. In addition, the energy volumes (WSA: wave spectrum area and BSA: buoy spectrum area) of each group were

arranged by integrating the area of the spectra in Table 4. Group 1 showed that SWH is equal to 0.7714 *m* and SBH to 1.6288 *m*, which is the smallest SBH value among those of the three groups. On the other hand, Group 3 showed that SWH is equal to 0.5935 *m*, but SBH to 1.8202 *m*. Such results can be confirmed through the groups' amplification rates (BSA/WSA): for Group 1, about 4.3-fold; Group 2, 5.18-fold; and Group 3, about tenfold, which was the largest. As shown in Figs. 8-10, the larger the incident wave energy distribution around the natural frequency (ω_h = 1.17 *rad/sec*) of the power buoy, the greater the increase in the amplification rate. Such results directly show that the wave energy can be largely absorbed by the power buoy, if the buoy's natural frequency is positioned within the frequency-band that has a certain volume of energy within the incident wave spectrum, even in low depth, where the peak frequency of the designated sea area and the natural frequency of the power buoy cannot coincide.

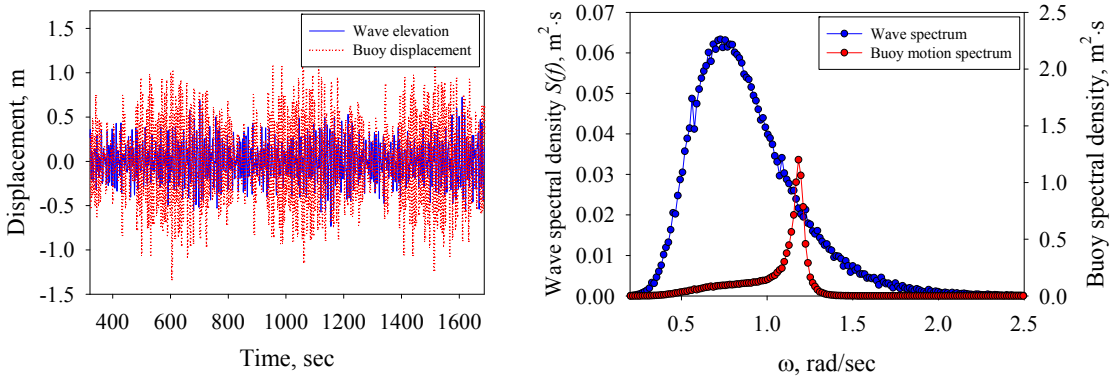

Fig. 8 Comparison of wave elevation and motion response of the buoy for Group 1: (a): time series, and (b): spectral density.

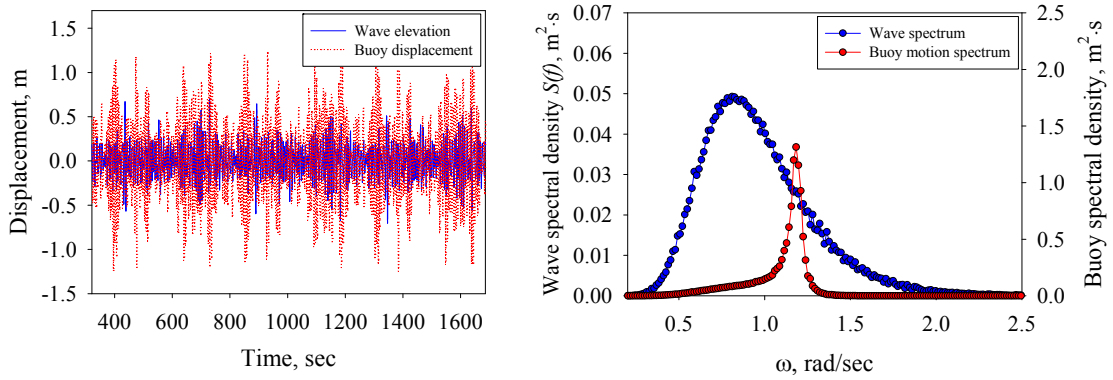

Fig. 9 Comparison of wave elevation and motion response of the buoy for Group 2: (a): time series, and (b): spectral density.

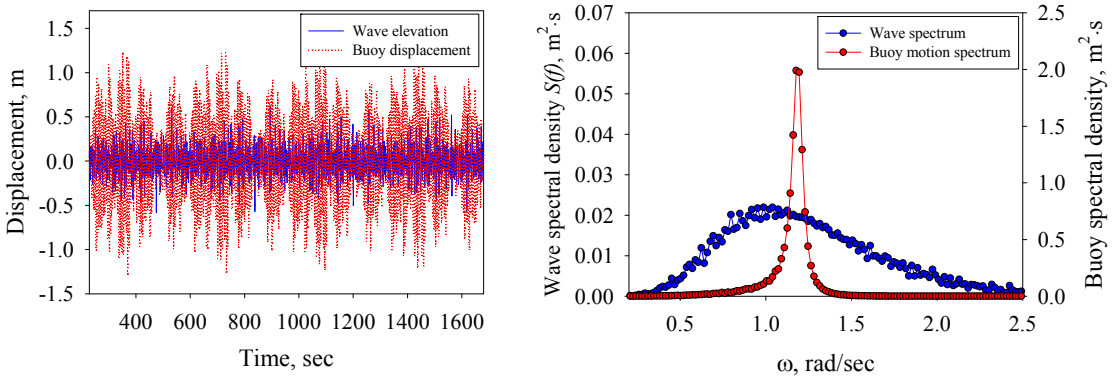

Fig. 10 Comparison of wave elevation and motion response of the buoy for Group 3: (a): time series, and (b): spectral density.

Table 4 Statistical properties of irregular waves and theirbuoy motion.

Group	SWH (significant wave height)	SBH (significant buoy height)	WSA (wave spectrum area)	BSA (buoy spectrum area)	BSA/ WSA
1	0.7714	1.6288	0.0404	0.1735	4.2972
2	0.6878	1.6598	0.0339	0.1756	5.1806
3	0.5935	1.8202	0.0225	0.2261	10.0591

CONCLUSION

The use of a resonance buoy to improve the efficiency of wave energy extraction is becoming popular. In this study, wave observation data were used as the input conditions, for the answer to the question as to whether or not the resonance effect was still effective in low depth, where a sufficient resonance draft that was appropriate to the peak frequency of the observed spectrum was not secured. Therefore, in this study, the heave motion characteristics of the buoy were investigated when the buoy is resonated with incoming waveswithhigher frequency than the peak frequency of the observed spectra in a real sea area. The higher resonant frequency corresponded to the case with a smaller buoy's draft. The following conclusions were obtained.

(1) A new expression utilizing the Probability Density Function (pdf), based on the Generalized Extreme Value (GEV) Cumulative Distribution Function (CDF) for the normal wave spectrum, was proposed.
(2) The circular cylinder-type buoy with a draft smaller than the resonance draft that corresponded to the peak frequency in the real sea area, produced larger heaving displacement spectra, than those of the entire incident wave energy.
(3) The amplification rates of the buoy varied, as the wave spectra changed by season.
(4) The changes in the wave spectra by season affected the areas of the heaving displacement spectra of the power buoys with the same dimensions, so many other buoys with different resonance drafts had to be installed, for smoother energy production.
(5) For the optimum design of the power buoy, the buoy motions must be analyzed, while considering the PTO-damping items in low depth.

ACKNOWLEDGEMENT

This work was supported by the New & Renewable Energy of the Korea Institute of Energy Technology Evaluation and Planning (KETEP) grant funded by the Korea government Ministry of Knowledge Economy (2010302007 0080).

REFERENCES

Budal, K. and Falnes, J., 1975. A resonant point absorber of ocean wave power. *Nature*, 256, pp.478-479.

Cho, I.H., Kim, M.H., Kweon, H.M., 2012.Wave energy converter by using relative heave motion between buoy and inner dynamic system, *Ocean Systems Engineering*, 2(4), pp.297-314.

Falnes J., 1999. Wave-energy conversion through relative motions between two single-mode oscillating bodies. *Journal of Offshore Mechanics and Arctic Engineering*, 121, pp.32-38.

French, M.J., 1979. A generalized view of resonant energy transfer. *Journal of Mechanical Engineering Science*, 21(4), pp.299-300.

French, M.J. and Bracewell, R.H., 1995. The systematic design of economic wave energy converters. *Proceedings of the 5th Offshore and Polar Engineering Conference, ISOPE,* Hague, Netherlands, 11-16 June 1995, pp.106-109.

Grilli, S.T., Grilli, A.R., Bastien, S.P., Sepe, R.B. and Spaulding, M.L., 2011. Small buoys for energy harvesting: Experimental and numerical model studies. *Proceedings of the 21th Offshore and Polar Engineering Conference, ISOPE,* Manui, Hawaii, USA, June 19-24 2011, pp.598-605.

Kweon, H.M., Koh, H.J., Kim, J.R. and Choi, Y.H., 2013a. Experimental study for the resonance effect of the power buoy amplitude, *Journal of the Korean Society of Civil Engineers*, 33(2), pp.585-594.

Kweon, H.M., Cho, H.Y. and Jeong, W.M., 2013b. Wave analysis and spectrum estimation for the optimal design of the wave energy converter in the Hupo coastal sea, *Journal of Korean Society of Coastal and Ocean Engineers*, 25(3), pp.147-153.